



PAPER

## Luminescence of YAG:Dy and YAG:Dy,Er crystals to 1700 °C

To cite this article: S W Allison *et al* 2020 *Meas. Sci. Technol.* **31** 044001

View the [article online](#) for updates and enhancements.

### You may also like

- [Particle-based temperature measurement coupled with velocity measurement](#)  
Satoshi Someya
- [Fiber-coupled phosphor thermometry for wall temperature measurements in a full-scale hydrogen gas turbine combustor](#)  
Patrick Nau, Andre Müller, Niklas Petry *et al.*
- [Characterization of YAG:Dy,Er for thermographic particle image velocimetry in a calibration cell](#)  
Ellen Hertle, Stefan Will and Lars Zigan

The banner features three distinct sections. On the left, a light green background contains the ECS logo (a stylized 'ECS' in a circle) and the text 'The Electrochemical Society' and 'Advancing solid state & electrochemical science & technology'. The middle section shows a photograph of an industrial robotic arm in a factory setting. The right section has a dark blue background with the text 'DISCOVER how sustainability intersects with electrochemistry & solid state science research' and a photograph of a woman looking at a colorful data visualization on a screen.

# Luminescence of YAG:Dy and YAG:Dy,Er crystals to 1700 °C

S W Allison<sup>1,3</sup>, D L Beshears<sup>1</sup>, M R Cates<sup>1</sup>, M B Scudiere<sup>1</sup>, D W Shaw<sup>2</sup> and A D Ellis<sup>2</sup>

<sup>1</sup> Emerging Measurements, Inc, Knoxville, TN, United States of America

<sup>2</sup> Department, General Electric, Greenville, SC, United States of America

E-mail: [steve.allison@emergingmeasurements.com](mailto:steve.allison@emergingmeasurements.com)

Received 20 June 2019, revised 14 October 2019

Accepted for publication 17 October 2019

Published 6 January 2020



CrossMark

## Abstract

Reported here are measurements aimed at development of high temperature luminescence-based fibre optic thermometry for temperatures up to at least 1700 °C. Cylindrical crystal samples of YAG:Dy(1%) and YAG:Dy(1.5%),Er(0.5%) were fabricated by the co-precipitation method. The optical system was comprised of Nd:YAG 355 nm laser light injected into one leg of flexible bifurcated optical fibre connected to a sapphire light pipe. The input end is water cooled and the sensing end is inside a furnace in proximity to the crystal. The emission originates from the Dy<sup>3+</sup> dopant. Decay times for the <sup>4</sup>I<sub>15/2</sub>–<sup>6</sup>H<sub>15/2</sub> (456 nm) transition in the YAG:Dy,Er host ranged from 856 ns at 1600 °C to 401 ns at 1700 °C. Signals taken at 10 °C intervals were clearly resolvable. Decay times appeared constant at 800 °C and below with average values of 863 μs for YAG:Dy and 734 μs for YAG:Dy,Er. Decay times from these two materials appear to converge to the same value at high temperatures. These results were achieved with laser excitation of 100 to 150 μJ. The results were compared to physical models both of which yielded reasonable empirical agreement for the limited amount of data. Thermal sensitivity determined from a multiphonon model shows that decay times change by 1% per degree at 1400 °C and 0.9% at 1700 °C. Dy emission was also detected at 405, 400 and 389 nm at 1575 °C and 1700 °C and showed the expected temperature dependence.

Keywords: luminescence, thermometry, yttrium aluminum garnet, dysprosium, erbium

(Some figures may appear in colour only in the online journal)

## 1. Introduction

The luminescence of phosphor powders, coatings, and crystals continues to be exploited for temperature, thermal history, and flow measurement. With respect to the important category of turbine engine diagnostics, much effort continues regarding measurement of extremely high temperatures. The present work describes measurements of such luminescence to 1700 °C, the limit of the test furnace. The eventual goal is development of a temperature probe to this temperature and higher.

### 1.1. Rationale

The mission statement of the Propulsion Instrumentation Working Group (PIWG) says it was formed ‘to address critical turbine engine test cell instrumentation, sensors and measurement technology to keep pace with the needs of turbine engine development’. PIWG is a consortium comprised of turbine engine original equipment manufacturers, small businesses, universities, national laboratories, AFRL, NASA, and DOE. One of the primary interests identified by the consortium involves sensors and systems for hot section measurements. ‘In the hot section, knowledge of gas temperature is necessary to estimate heat transfer to surfaces, combustion stoichiometry, and burner pattern factor...’ Control and health management of modern turbine engines depends on accurate sensing of physical quantities associated with the engine design and performance, such as

<sup>3</sup> Author to whom any correspondence should be addressed.

temperature, pressure, vibration, component degradation, and erosion, as well as possible problem areas for health monitoring. Sensors in use today are prone to degradation arising from oxidation, erosion, and contamination because of the high-temperature and corrosive gases in turbine engine environments. An advanced method of making these temperature measurements, using fiber optics coupled to high-temperature luminescent material could serve the goal of achieving efficient, safer, and longer duty cycle turbine engine designs. Better sensors will allow for operation closer to material temperature limits where engine performance is higher and more efficient. The present work quantifies signal levels and establishes temperature sensitivities for a fibre optics based design in the critical region of our present interests, 1600 °C–1700 °C.

### 1.2. Luminescence thermometry background

Luminescence-based thermometry makes use of temperature dependent luminescence properties of many types of materials [1]. A prime example are thermographic phosphor materials for which there is a large body of literature [2–7]. Other examples include rare-earth doped optical fiber [8], phosphor impregnated silicone patches [8–12], and discrete crystals [13, 14]. Regardless of which of these is involved, the methodology is similar. That is, when illuminated by some means such as a laser, the brightness, spectral content, and temporal behaviour of the luminescence changes as a function of temperature.

There are several categories of temperature sensors based on luminescence. Thermometry using phosphors has been one of the main implementations exploiting luminescence temperature dependence. Another has involved placing a phosphor or a crystal at the end of an optical fiber in order to achieve the optical analog of a thermocouple. The first commercial device by Luxtron used a phosphor at the end of a fiber. Others, for example Bossleman [14], used a ruby or YAG:Cr crystal. As time has progressed there have been many efforts to achieve higher temperature measurement capability. One of the reasons that YAG is of interest is because of its high melting point which is  $1940 \pm \text{°C}$  [15]. Zhang *et al* achieved a monolithic doped fiber sensor using the laser heated pedestal growth method. They first grew a YAG single crystal then began adding Er for the final 5 mm. Thus the luminescent end was of YAG:Er [16]. They demonstrated measurement capability to just over 1000 K, which was limited by their heating capability at that time. In follow on work by Kennedy and Djeu, decay based temperature measurement to 1600 °C was achieved using YAG:Yb material. [17, 18] The technology led to development of a commercial product, the product line called Opto Temp 2000 by Micromaterials [19]. The goal of the present effort is to develop a temperature probe for temperature measurement of flows in the hot section of turbine engines. It is thought that using the bulk crystalline form of the YAG materials would have the potential advantages of robustness and higher signal levels over the phosphor powder form.

There are several attributes of the luminescence that may be exploited for temperature sensing. For Dy materials, below about 1000 °C, the ratio of distinct emission lines is used. The most commonly used parameter above about 1000 °C is the

decay time. For this, the luminescence is excited by a short pulsed high energy burst of laser light. The resulting emission will persist, decaying at a characteristic rate which is a function of temperature.

### 1.3. Previous very high temperature work

The present effort concerns high temperature testing of a probe for extremely high temperatures. What is the limit in temperature for luminescence thermographic materials? What are the choices for very high temperatures? This is an active area of investigation. The material with the longest history in this field is YAG:Dy. It was first identified and tested by Goss *et al* [20]. Later, Lewis *et al* made decay measurements to nearly 1400 C [21]. Cates *et al* made laboratory measurements of YAG:Dy phosphor powder to 1700 °C in a laboratory furnace [22]. Subsequent efforts have involved variations on this material. Jaber *et al* obtained spectra of YAG:Dy and YAG:Dy,Er to 1800 °C, the Er acting as a sensitizer to the Dy [23]. Other co-dopants in YAG:Dy in related work more recently explored were Tm, Tb, and Pr. It was established, in tests to 1600 K, that luminescence could be enhanced by 30% with Tb and Pr also as sensitizers [24, 25]. A different approach was taken by Kwong *et al*. They substituted  $\text{B}^{3+}\text{-N}^{3-}$  into the YAG host to produce YABNG:Dy. This material exhibited stronger luminescence and a quenching onset of 100 °C higher than YAG:Dy. The new material was tested only to 1227 °C (1500 K) and comparisons made of signal ratios [26, 27]. Finally, as an example of a measurement application, Nau *et al* measured wall temperatures of a combustor using thermographic phosphors, achieving a temperature stated as 1800 K [28].

### 1.4. Explanation of approach

The motivating objective is development of a temperature sensor for high temperature situations such as in turbine engine combustors. Several requirements result from this objective. In anticipation of the need for making tight turns inside and in the vicinity of such machinery, the first requirement necessitates flexible small diameter optical fibre for both delivery of excitation light and the return luminescence. This places a limit on laser fluence since it must be kept below the optical fibre surface damage threshold. Another requirement is the use of a sapphire light pipe with water cooling on the input end for transitioning to the highest temperatures. This allows connecting flexible fibre that has limited temperature capability to the cool end of the sapphire.

The first goal of the measurements was to quantify signal levels from 1500 °C to 1700 °C, the range of anticipated applications, with the intent to establish the feasibility of achieving 10 °C resolution. The second was to quantify blackbody emission in relation to the fluorescence. Cates *et al* [22] encountered large blackbody emission at the highest temperatures. Blackbody manifests as a constant background signal. For low levels it is adequate to subtract this constant value from the received signal before processing. But, at the highest temperatures this is not suitable because, for sufficiently high signal levels, detectors have difficulty responding

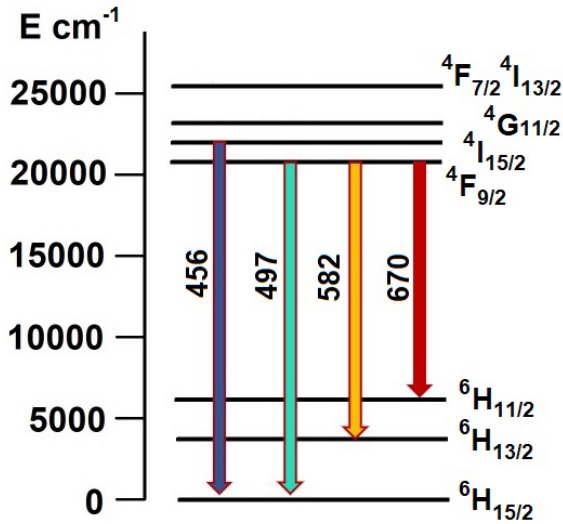


Figure 1. Simplified energy level diagram for Dy<sup>3+</sup> in YAG.

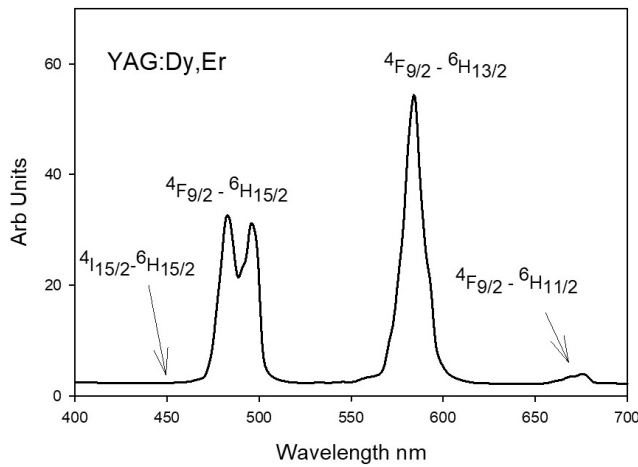


Figure 2. Spectrum of YAG:Dy,Er crystal for 355 nm excitation.

linearly. Thus, it is important to understand and quantify this phenomenon.

Figure 1 is a simplified energy level diagram illustrating the major emission lines of Dy<sup>3+</sup> in the visible. Figure 2 is a low resolution spectrum at ambient temperature, 24 °C, of a YAG:Dy,Er crystal showing the main emission bands excited by 355 nm. A StellarNet Blue-Wave spectrometer was used. At this resolution, no difference could be discerned between YAG:Dy and YAG:Dy,Er samples, thus there was no significant emission from Er bands at room temperature. Also note that, as is common, the signal level of the Dy emission around 456 nm, ⁴I<sub>15/2</sub>-⁶H<sub>15/2</sub>, is too weak for detection. However, this band grows and at high temperatures is brightest. Blackbody emission at 1700 °C is greater by a factor of ten for the 575 nm band than for the 456 nm band. Because of this as well as time limitations, no measurements of the bands at 575 and 670 nm were conducted.

### 1.5. Temperature dependence and non-radiative relaxation

Consider that an electron in the excited state has two possible paths to deexcitation. One is to emit a photon, the other is to relax non-radiatively. The rate of deexcitation  $W$  is the sum

of the radiative rate,  $W_r$ , and the non-radiative rate,  $W_{nr}$ . The measured decay time,  $\tau$ , is simply  $1/W$ . The unquenched low temperature decay time, a constant, is  $\tau_0 = 1/W_r$ . Therefore,

$$\tau = (W_r + W_{nr})^{-1} = \left( \frac{1}{\tau_0} + W_{nr} \right)^{-1}. \quad (1)$$

There are two types of thermal relaxation processes that may be responsible for the temperature dependence of  $W_{nr}$  [29]. Thermal relaxation for both Dy and Er doped materials is usually ascribed to a multiphonon process. For example, Eldridge (30) provides detailed use of this model for characterizing Y<sub>2</sub>O<sub>3</sub>:Er emission. Heyes [31] applies the model to YAG:Dy. Dramicanin [1] and Brites [7] also give good descriptions in the context of luminescence thermometry. According to this model, de-excitation occurs by the simultaneous emission of  $p$  phonons of energy  $\hbar\omega$  between electronic levels separated by an energy gap of  $\Delta E_m$ . In which case

$$p = \frac{\Delta E_m}{\hbar\omega}. \quad (2)$$

Heyes, for example, provides the following relations

$$W_{nr}^p(T) = W_{nr}^p(0) [n + 1]^p. \quad (3)$$

Where, with  $k$  as Boltzmann constant,  $n$  is

$$n = \left[ \exp\left(\frac{\hbar\omega}{kT}\right) - 1 \right]^{-1} \quad (4)$$

which leads to

$$W_{nr}^p(T) = W_{nr}^p(0) \left[ \frac{1}{1 - \exp\left(-\frac{\Delta E_m}{p k T}\right)} \right]^p. \quad (5)$$

By substitution to equation (1) the result is

$$\tau(T) = \frac{1}{\frac{1}{\tau_0} + W_{nr}^p(0) \left[ \frac{1}{1 - \exp\left(-\frac{\Delta E_m}{p k T}\right)} \right]^p}. \quad (6)$$

Heyes estimated  $W_{nr}^p(0) = 2.7 \cdot 10^{-3} \text{ s}^{-1}$  and  $\Delta E_m = 8000 \text{ cm}^{-1}$  for the ⁴F<sub>9/2</sub> to ⁶F<sub>1/2</sub> transition for YAG:Dy. A fit to available data that extended only up to 1200 °C yielded a value of  $p$  of 20.

The other model is from Mott-Seitz theory. For that model, in consideration of a configurational coordinate picture, the parabola of the excited state intersects with the ground state or a charge transfer state which in turn connects to ground state, nonradiatively. The energy difference between the excited electronic state minimum and the intersection is  $\Delta E_c$ . When the thermal distribution in the excited state reaches this level, the energy crosses over to the adjacent state and hence de-excites nonradiatively. As an example, Fonger and Struck [32] used this approach to describe thermographic phosphors such as La<sub>2</sub>O<sub>2</sub>S:Eu. For this, decay time is expressed as:

$$\tau(T) = \frac{1}{\frac{1}{\tau_0} + a \cdot \exp\left(-\frac{\Delta E_c}{kT}\right)}. \quad (7)$$

Where  $a$  is a rate constant with units  $\text{s}^{-1}$ .

## 2. Experimental

### 2.1. Materials

The YAG:Dy(1.0%) and YAG:Dy(1.5%),Er(0.5%) crystals were obtained from World-Lab Co. Ltd of Nagoya, Japan.

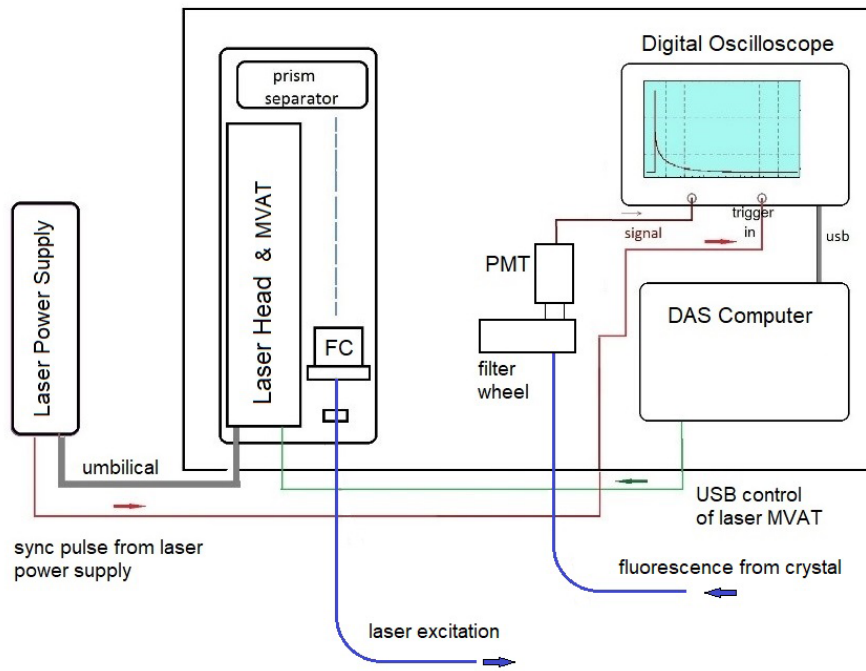


Figure 3. Block Diagram.

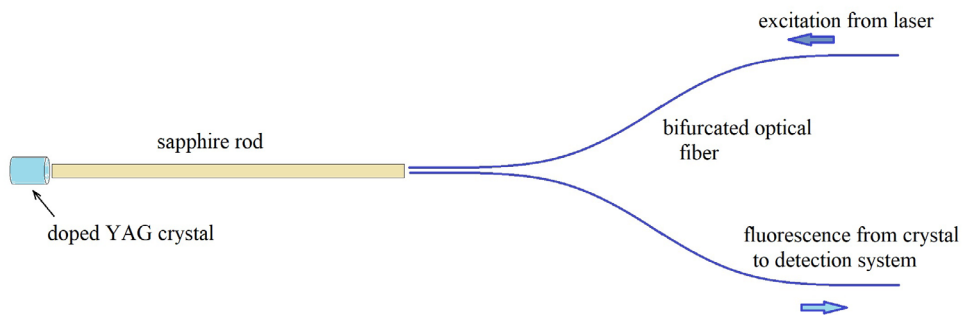


Figure 4. Optics of crystal illumination and signal capture.

They were fabricated by the co-precipitation method [33]. This method purports to yield a material for which the dopant ions are uniformly and consistently distributed.

The dimensions of the crystals were 5 mm long by 3.5 mm diameter. First the ceramic powder is made in a batch and placed in a mould long enough to make four crystals. After processing, the resulting crystal is removed, cut into four pieces, then machined and polished to the specified dimensions.

## 2.2. Test setup

**2.2.1. Light delivery system.** Figure 3 shows a block diagram of the major test setup components. The laser was a Q-switched Nd:YAG Laser System with 2nd, 3rd, and 4th Harmonic Generation manufactured by Quantel Corporation. It was a Big Sky Laser Ultra Series PN ULC8HC11. It incorporated an MVAT component for precise control of output amplitude without modifying beam profile. The laser output is at 355 nm, with a repetition rate 0 to 20 Hz, and pulsewidth about 5 ns. The Prism Separator in the figure consists of a dispersing prism and turning mirror. It separates the co-linear beams that

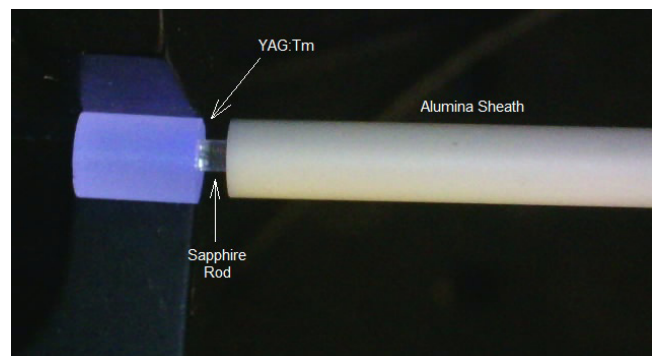
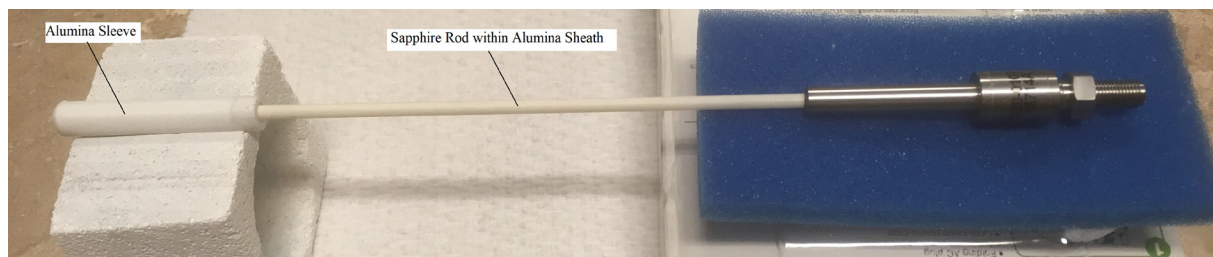


Figure 5. Luminescing YAG:Tm crystal and sapphire probe.

emerge from the laser head. Adjustable knobs of the mirror allow alignment of the desired beam, in this case the one at 355 nm, to a fiber coupler assembly, FC. Between them is a 355 nm bandpass filter and its holder. This additional filtering is needed to prevent spurious emission, possibly from the laser flashlamp, from interfering with the fluorescence. This is especially noticeable for signals with short decays. Once the laser parameters such as the flashlamp energy, Q-switch



**Figure 6.** Photograph of Sapphire Probe.

settings, and repetition rate are set, the laser energy levels are controlled from the data acquisition system through a Putty program. A Thorlab Model PW200 Laser Power monitor measured laser energy. Inside the FC fixture is a lens that focuses the light to the entrance plane where a fiber optic SMA connector is affixed. The light beam direction is adjusted to center it within the SMA aperture. Then a  $2 \times 1$  bifurcated fiber is attached. This is illustrated in figure 4 (not to scale). It is comprised of two 600 micron fibers; at one end the two are side-by-side within an SMA ferrule. The other ends are free. One end, the delivery fiber, is attached to the FC and the lens is adjusted to maximize the amount of laser light injected into it. The two-fiber output end connects to a 1.25 mm diameter sapphire rod. The sapphire rod guides the excitation light to the crystal where fluorescence is generated. The laser energy emerging from the sapphire ranged from 100 to 150 microjoules. This corresponds to a fluence of  $0.012 \text{ J cm}^{-2}$ . This is somewhat below  $0.030 \text{ J cm}^{-2}$  used by Hertle *et al* [25] in their investigations with certain YAG:Dy phosphor powders. They considered the latter value as sufficiently low to avoid effects of laser fluence. An additional factor is the depth of penetration of the light. Lupei *et al* [34] determined an absorption crosssection for YAG:Dy of  $9 \times 10^{-21} \text{ cm}^2$  at the band peak of 353 nm at 300 K. By approximating the density the same as YAG,  $4.56 \text{ gm cm}^{-3}$ , this corresponds to an attenuation coefficient of  $1.26 \text{ cm}^{-1}$ . The reciprocal indicates a penetration depth of about 8 mm. Since the laser fluence is spread over this relatively large volume, it is expected that the role of fluence is nil. A fraction of the fluorescence generated in this manner enters the sapphire rod and is transmitted to the receiver fiber which conveys it to the detection and analysis system.

**2.2.2. Sapphire probe.** Figure 5 is a photograph of a luminescing YAG:Tm crystal used in some preliminary testing as excited by light conveyed by the sapphire rod. The rod within an alumina pipe and with stainless steel fixturing at the input end is what is termed as a sapphire probe. The input side is within a stainless steel sleeve and has an SMA fiberoptic connector. This is depicted in figure 6. An alumina tube extends from the stainless steel. Within the alumina tube is the sapphire rod which protrudes 1 mm from the alumina. In this photo, an alumina sleeve contains the crystal. The YAG crystal, sapphire and alumina will each survive temperatures in excess of  $1900 \text{ }^\circ\text{C}$ . The initial probe, was kindly provided by J I Eldridge of NASA Glenn and is of his design. The alumina extension was 16 cm in length. This is a sufficient length for a  $1000 \text{ }^\circ\text{C}$  furnace used in some preliminary testing. Subsequently a longer version for

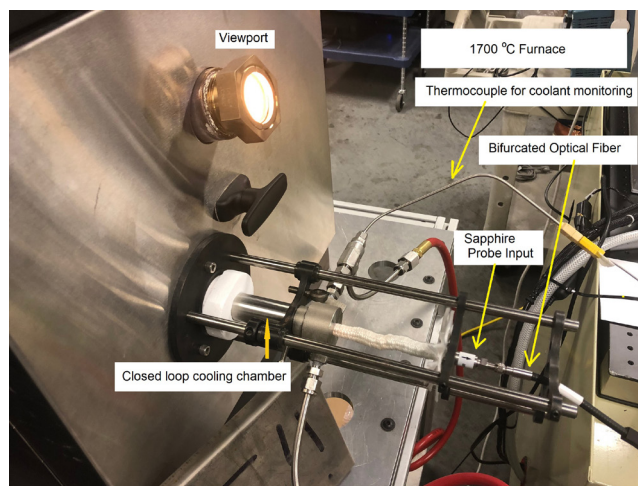


**Figure 7.** Furnace, cooling jacket, sapphire probe and bifurcated fiber.

which the alumina portion was 33 cm was procured as it was necessary for use with the  $1700 \text{ }^\circ\text{C}$  furnace.

The assembly shown in figure 6 was partially encased by a tubular closed loop cooling chamber, as seen in figure 7, in order to protect the lower temperature components in the probe from high temperatures in the furnace. A 1700 Series Rapid Temp lab furnace and associated controller, both manufactured by CM Furnaces, were used for the testing. This is also seen in figure 7.

**2.2.3. Detection and analysis.** The signal carrying leg of the bifurcated fibre connects to a manually rotatable filter wheel. It allows up to six different filters. Behind this is a lens which images the filtered signal onto a photomultiplier tube (PMT) detector, Hamamatsu H10721-110 with 300–650 nm sensitivity. The PMT signal is displayed and digitized by a Tektronix MSO 5404 oscilloscope with  $50 \Omega$  termination. A USB connection is made to a laboratory computer. An EMCO commercial program called EXP captures and analyses the data. This consists of pairs of voltage ( $I$ ) and time values ( $t$ ). As is often the case for phosphor thermometry, the data is fit to an exponential curve with an offset.

$$I = I_0 e^{-\frac{t}{\tau}} + b. \quad (8)$$

Figures 8 and 9 are two plots of a representative signal at  $1600 \text{ }^\circ\text{C}$ , the latter being the log view. There are two vertical cursors, medium dash lines, positioned before the fluorescence signal. The mean value between them determines the background level,  $b$ , which in this case is mostly blackbody

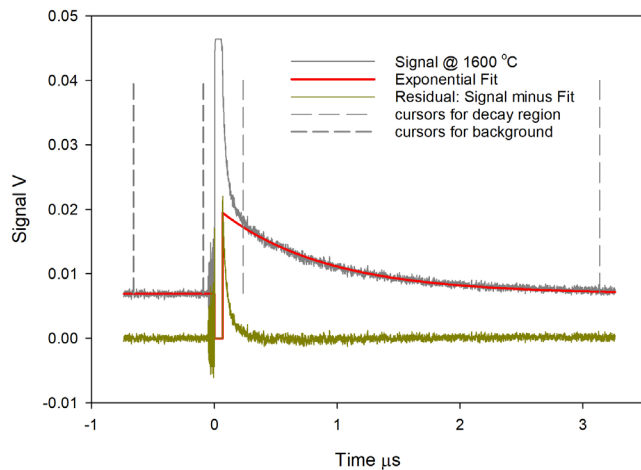


Figure 8. Signal at 1600 °C.

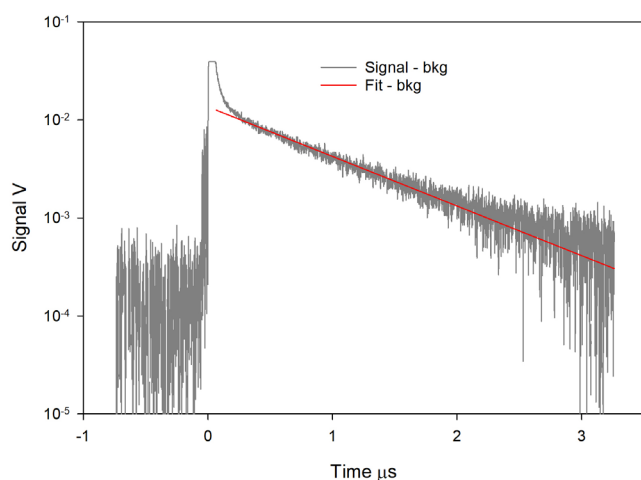


Figure 9. Log plot of 1600 °C signal.

emission. The analysis takes this into account. The early portion of the signal contains leakage of the laser through the filter and then a rapid decay component of unknown origin though commonly seen that is ignored in the analysis. Two long-dash vertical lines correspond to cursors placed within the fluorescence region, the left red cursor is positioned after the short decay component and the right red cursor usually is placed to the far right to the time limit unless there is too much noise. Only the region between the cursors is analysed to determine decay time,  $\tau$ . The grey curve of figures 8 and 9 is the actual data for YAG:Dy,Er. The red curve is the single exponential fit obtained by the software algorithm. The value of the decay time determined for these cursor settings was 856 ns. The dark yellow curve is a plot of the single exponential curve fitted to the data subtracted from the actual and helps to visualize where to place the cursors. This dark yellow trace is termed the residual curve. It is the signal minus the fit. Note that the magnitude of this deviation from the single exponential fit is small within the segment bounded by the cursors, which is after about the first 300 ns. It is desirable to have a single exponential fit as such are simpler to analyse. Though high dopant levels will up to a point increase signal levels, they often result in signals that poorly fit a single exponential.

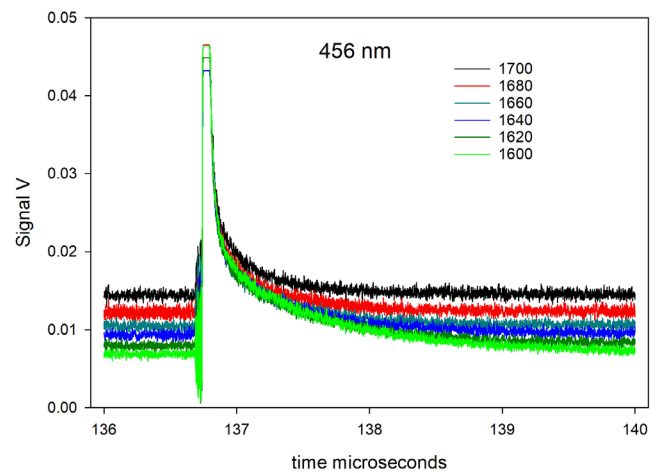


Figure 10. Plot of Signals from 1600 to 1700 °C, YAG:Dy,Er at 456 nm.

It appears that the choice of 1.5% for Dy and 0.5% Er for the present effort was satisfactory in this regard. It could also be that the co-precipitation method of fabrication may play a positive role in this as well.

### 3. Results

#### 3.1. Signals versus temperature 456 nm

The most important emission band for high temperature thermometry for Dy based phosphors is the  ${}^4I_{15/2}$  to  ${}^6H_{15/2}$  transition. Emission from this band ranges from about 450 to 460 nm and broadens with temperature. It is weak at room temperature so that sometimes it is not even detected in spectra. However, emission within this band does increase with temperature because it is fed by thermalization from the  ${}^4F_{9/2}$  state which is approximately  $1000\text{ cm}^{-1}$  below it. It increases to a maximum around 1000 °C. The room temperature decay time of this state is about 20  $\mu\text{s}$ , however what is detected will be of longer persistence due to being fed from the longer lived  ${}^4F_{9/2}$  state.

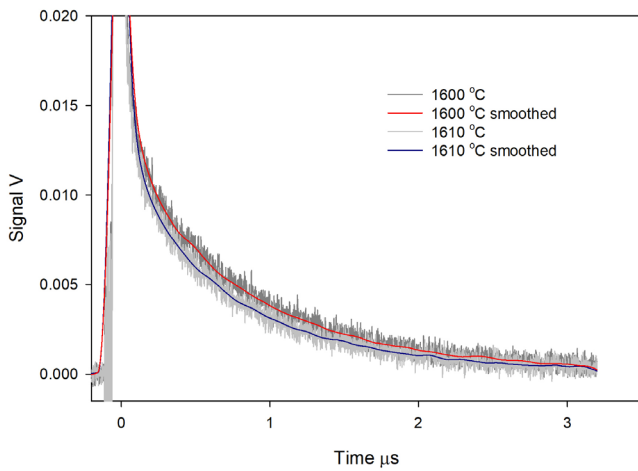
Tests runs were made with YAG:Dy and YAG:Dy,Er crystals. Though data was taken in 10 °C intervals, for clarity, figure 10 shows waveforms in 20 °C increments for the double-doped sample from 1600 °C to 1700 °C. Clearly the decay time decreases. The decay time of YAG:Dy,Er at 1700 °C is 401 ns. Note that the baseline of the scans increase with temperature owing to blackbody emission within the bandpass of the filter, as expected. One goal was to demonstrate feasibility of 10 °C resolution. Visually this is depicted in figure 11 where the signals are quite distinct. The measured decays are 856 and 787 ns at 1600 °C and 1610 °C, respectively, a change of about 8% in this 10 °C span.

#### 3.2. Decay time versus temperature for 456 nm

Figure 12 combines decay time versus temperature data from both YAG:Dy and YAG:Dy,Er. It is seen that the decay time appears to be constant up to 800 °C. The average value of the decay time up to and including that temperature is 734

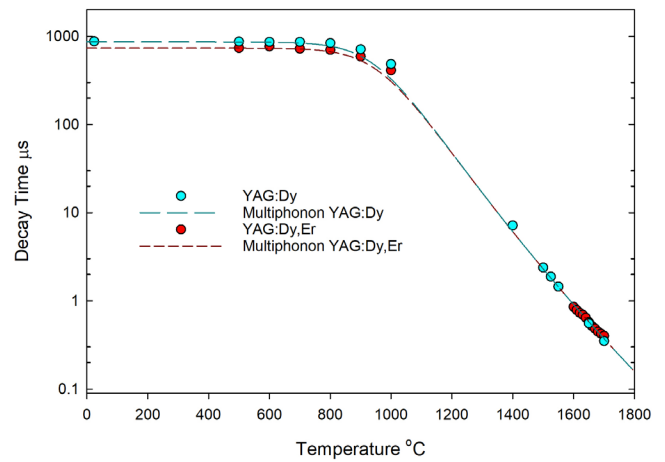
**Table 1.** Model fit results.

	Multiphonon model				Mott–Seitz model		
	$\tau_0$	$\Delta E_m$	$p$	$W_{nr}^p(0)$	$\tau_0$	$\Delta E_c$	$A$
YAG:Dy	863 $\mu\text{s}$	8000 $\text{cm}^{-1}$	20 phonons	$3.1 * 10^6 \text{ s}^{-1}$	863 $\mu\text{s}$	22 600 $\text{cm}^{-1}$	$3.9 * 10^{13} \text{ s}^{-1}$

**Figure 11.** Comparison of signals at 1600 °C and 1610 °C, YAG:Dy,Er at 456 nm.

$\mu\text{s}$  for YAG:Dy,Er and 863  $\mu\text{s}$  for YAG:Dy. These values are taken to be the unquenched decay time  $\tau_0$  discussed in the section on models. At 900 °C and above, decay times decrease as temperature increases. There is a gap in the data from 1000 °C to 1400 °C because there was not sufficient time during the test opportunity to address this region. From about 1400 °C to 1700 °C, decay times for the two different materials converge. For their tests which were to about 1700 K, this was also observed by Hertle *et al* [35] for YAG:Dy (2%) and YAG:Dy (2%), Er(1%) and for these same dopants in  $\text{Y}_2\text{SiO}_5$ .

The lines through the data in this plot were derived from the multiphonon model discussed earlier and fit very well in the high temperature region. This model depends on four parameters, unquenched decay time  $\tau_0$ , energy gap  $\Delta E_m$ , the number of phonons,  $p$ , and the nonradiative decay rate  $W_{nr}^p(0)$ . Heyes [31] gives 8000  $\text{cm}^{-1}$  as the energy gap,  $2.7 * 10^{-3}$  for the nonradiative decay rate, and  $p = 20$  for the number of phonons transitioning the gap. Whereas Heyes was fitting to a curve up to 1200 °C our work covers an additional 500 °C. The nonradiative decay rate in the present work was three orders smaller. According to this model, quenching should commence at a slightly lower temperature than what was observed. Table 1 has the parameters of the fits for both the multiphonon and Mott–Seitz models. The degree to which the Mott–Seitz equation fits with the data is depicted in figure 13 for YAG:Dy. The results for YAG:Dy,Er were similar. By arbitrarily adjusting the activation energy  $\Delta E_c$  and the rate constant,  $a$ , this model gives an adequate empirical fit at low and high temperatures but indicates a slightly higher onset of quenching than what was observed. This is a merely empirical fit. The activation energy and rate constant might not correspond with the spectral properties of this material.

**Figure 12.** Decay time versus temperature, 24 °C to 1700 °C, at 456 nm.

Following Eldridge [30], the relative thermal sensitivity,  $S_{rel}$ , of decay time for the multiphonon model is

$$S_{rel} = \frac{1}{\tau} \frac{d\tau}{dT} \approx \frac{-\Delta E_m \cdot n}{kT^2}. \quad (9)$$

Where  $n$  is defined by equation (4). This yields 1% change in decay time per degree at 1400 °C and 0.9% at 1700 °C.

### 3.3. Other emission bands

Some measurements were made of the band  ${}^4\text{F}_{9/2}$ – ${}^6\text{H}_{15/2}$  at 486 nm. Weak signals of roughly the expected decay times were observed at 1400 °C and 1500 °C. A cursory investigation of other emission bands was made using bandpass filters that were available. The filters were of 10 nm bandwidth centered at 405, 400, and 389 nm. There are higher lying states of Dy which emit weakly if at all at room temperature. These are  ${}^4\text{G}_{11/2}$  at 425 nm and several closely spaced levels:  ${}^4\text{F}_{7/2}$ ,  ${}^4\text{I}_{13/2}$  at 387 nm [35, 36]. But also, there are Er bands in the vicinity including the transitions  ${}^2\text{H}_{9/2}$  to  ${}^4\text{I}_{15/2}$  near 405 nm and  ${}^4\text{G}_{11/2}$  to  ${}^4\text{I}_{15/2}$  around 385 nm [37]. Given that these features will broaden at these high temperatures we are not prepared to assert an identification of the states from which emission is occurring. It could well be that it is a result of thermalization from the  ${}^4\text{F}_{9/2}$  state of Dy since the decay times match the Dy. Regardless of origin, figure 14 depicts signals from 405 and 389 at 1575 °C. Signals were observable to 1700 °C. Eldridge [30] describes how emission decay measurements from  $\text{Y}_2\text{O}_3$  solely activated by Er can be useful for wide ranging temperature sensing. Careful attention is given to the modelling of the emission in that paper. It may be concluded that future investigations could give more attention to the role of Er in the double-doped material as it may provide

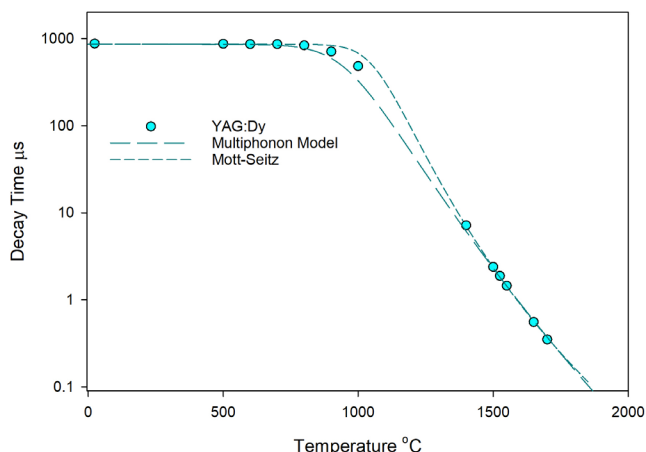


**Figure 13.** Decay time versus temperature for YAG:Dy with multiphonon and Mott–Seitz fits to the data.

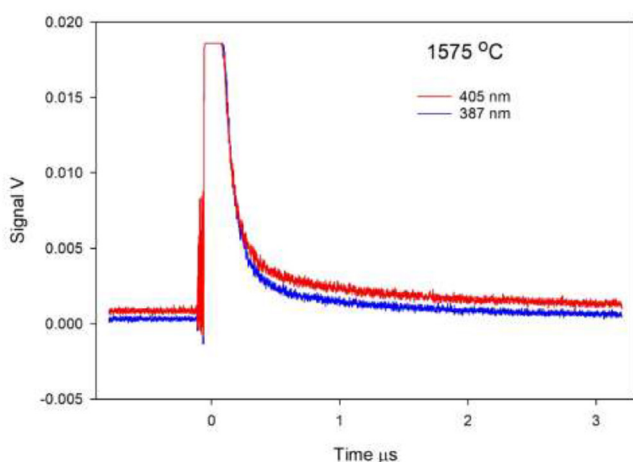


**Figure 14.** Signals at 405 and 387 nm at 1575 °C.

additional emission states for temperature measurement. This could be particularly the case for different excitation wavelengths than used here.

### 3.4. Blackbody emission

Some background blackbody emission is detected within the bandpass of the filters. It appears to follow the expected temperature dependence. It is taken as the value of the signal before the laser excitation. Figure 15 shows both decay times and blackbody emission determined from the 456 nm data. The blackbody emission is compared to Planck’s law of spectral irradiance and appears to match with that as expected.

### 3.5. Exposure to high temperature

Given that 1700 °C is not far from the melting temperature of 1940 °C, the possible effects of exposure may be considered. For example, ion diffusion if it occurs could affect the measurements. The YAG:Dy sample was tested the first day for about five hours during which the temperature ranged from 1400 °C to 1700 °C. The second day a signal was acquired at room temperature, 24 °C, and compared with that from an unexposed crystal

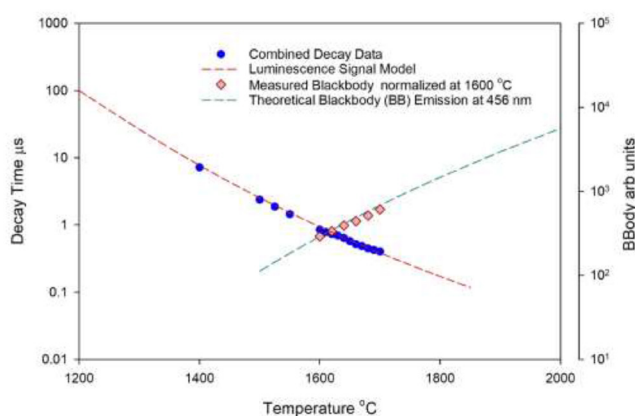


**Figure 15.** Combined plot of decay data and blackbody at 456 nm. Dashed line moving up to the right is blackbody model.

from the same batch. The determined decay times were 878 and 871 ms for unexposed and exposed samples, respectively. Because there is little difference between the two signals, only about 1%, it appears the crystal was not significantly affected by this duration and history of exposure. It is understood that additional investigation of the effect of long term exposure to these temperatures is needed for establishing viability for long term temperature measurement with these materials.

## 4. Conclusions

It was established that signal levels of the 456 nm band were sufficient to attain at least a 10 °C resolution. This was achieved with 100 to 150 microjoules of laser excitation. Both the excitation delivery and luminescence receiving fibers were 600 μm diameter. This energy level could be conveyed by even smaller fiber having greater flexibility in the future if needed for reaching difficult to access locations. It may also indicate that less expensive light sources could be viable.

Since blackbody emission is also detected in the course of observing the luminescence, it appears that both blackbody emission and crystal luminescence may be used for cross calibration and for extending to higher temperatures where the luminescence signals may be low. Future investigations could address the conditions for which this may be applicable and how it might compare with other pyrometry methods mentioned in the literature.

The application here intends to use discrete crystals. It is possible however to ground this material in order to create particles suitable for flow measurements. Perhaps the method of fabrication may result in particles having distinguishing features from phosphor particles prepared by other means.

Future work will seek to fill in decay time values for lower temperatures than reported here for these materials. Tests will be conducted over longer periods to uncover any annealing or diffusion effects.

### Note added in proof

While making the final edit to this manuscript, the authors became aware of a recent significant publication. Anderson

et al [38] developed what they term an optical thermocouple comprised of a thin YAG:Dy film, ranging from 0.5 to 13  $\mu\text{m}$  thickness, laser-deposited onto a sapphire fibre. The photoluminescence was excited by Q-Switched Nd:YAG laser at 355 nm. They used the ratio method to sense temperatures to 1773 K. It is noteworthy that they detect luminescence to 2033 K. Using a pulsed CO<sub>2</sub> laser as a heating source, they demonstrated high speed temperature measurement to 80 kHz. Diagnostics of explosive fireballs and turbulent flow are stated applications. This is an important addition to the field and is complementary to the present work where higher temperature measurement was demonstrated owing to the larger emitting volume of the YAG:Dy crystals. Response time was not addressed in the present effort but is expected to be considerably less than for the thin film configuration.

## Acknowledgments

The authors wish to acknowledge and thank Dr Jeff Eldridge of NASA GRC for loan of one of the sapphire probes and helpful conversations regarding Er<sup>3+</sup> spectral characteristics and the multiphonon model.

## ORCID iDs

S W Allison  <https://orcid.org/0000-0002-5887-5403>  
 D L Beshears  <https://orcid.org/0000-0001-9167-3152>  
 M R Cates  <https://orcid.org/0000-0002-5922-7731>

## References

- [1] Dramićanin M 2018 *Luminescence Thermometry: Methods, Materials, and Applications* (Duxford: Woodland Publishing)
- [2] Allison S W and Gillies G T 1997 Remote thermometry with thermographic phosphors: instrumentation and applications *Rev. Sci. Instrum.* **68** 1–36
- [3] Khalid A H and Kontis K 2008 Thermographic phosphors for high temperature measurements: principles, current state of the art and recent applications *Sensors* **8** 5673–744
- [4] Chambers M D and Clarke D R 2009 Doped oxides for high-temperature luminescence and lifetime thermometry *Ann. Rev. Mater. Res.* **39** 325–59
- [5] Aldén M, Omrane A, Richter M and Sarnier G 2011 Thermographic phosphors for thermometry: a survey of combustion applications *Prog. Energy Combust. Sci.* **37** 422–61
- [6] Brübach J, Pflitsch C, Dreizler A and Atakan B 2013 On surface temperature measurements with thermographic phosphors: a review *Prog. Energy Combust. Sci.* **39** 37–60
- [7] Brites C D S, Millan A and Carlos L D 2016 Lanthanides in luminescent thermometry *Handbook on Physics and Chemistry* vol 49 (Amsterdam: Elsevier) ch 281 pp 339–427 (<https://doi.org/10.1016/bs.hpcr.2016.03.005>)
- [8] Allison S W 2019 A brief history of phosphor thermometry accepted for publications in measurement *Sci. Technol.* **30** 072001
- [9] Wade S A, Collins S F and Baxter G W 2003 Fluorescence intensity ratio technique for optical fiber point temperature sensing *J. Appl. Phys.* **94** 4743
- [10] Parajuli P, Allison S W and Sabri F 2017 Spincoat-fabricated multilayer PDMS-phosphor composites for thermometry *Meas. Sci. Technol.* **28** 065101
- [11] Fontenot R S, Allison S W, Lynch K J, Hollerman W A and Sabri F 2016 Mechanical, spectral, and luminescence properties of ZnS:Mn doped PDMS *J. Lumin.* **170** 194–9
- [12] Mitchell K E, Gardner V, Allison S W and Sabri F 2016 Synthesis and characterization of flexible thermographic phosphor temperature sensors *Opt. Mater.* **60** 50–6
- [13] Grattan K T V and Zhang Z Y 1995 *Fiber Optic Fluorescence Thermometry* (London: Chapman and Hall) pp 335–76
- [14] Bosselmann T, Reule A and Schroeder J 1984 Fiber-optic temperature sensor using fluorescent decay time *Proc. SPIE* **514** 151
- [15] Caslavsky J L and Viechnicki D J 1980 Melting behaviour and metastability of yttrium aluminium garnet (YAG) and YAlO<sub>3</sub> determined by optical differential thermal analysis *J. Mater. Sci.* **15** 1709
- [16] Zhang Z, Herringer J H and Djeu N 1997 Monolithic crystalline fiber optic temperature sensor *Rev. Sci. Instrum.* **68** 2068–70
- [17] Kennedy J L and Djeu N 2002 Operation of Yb:YAG fiber optic temperature sensor up to 1600 °C *Sens. Actuators A* **100** 187
- [18] Kennedy J L 2006 Investigations of fiber optic temperature sensors based on Yb:Y<sub>3</sub>Al<sub>5</sub>O<sub>12</sub> *PhD Dissertation* University of South Florida
- [19] MicroMaterials Inc. 2019 Fiber optic temperature sensors
- [20] Goss L P, Smith A A and Post M E 1989 Surface thermometry by laser-induced fluorescence *Rev. Sci. Instrum.* **60** 3702–6
- [21] Lewis W, Turley W D, Borella H M and Noel B W 1990 Noncontact thermometry in excess of 2500 F using thermographic phosphors *Proc. 36th Int. Instrumentation Symp.* (Research Triangle Park, NC: ISA) pp 23–7
- [22] Cates M R, Allison S W, Jaiswal S L and Beshears D L 2003 YAG:Dy and YAG:Tm fluorescence to 1700 °C *Proc. of the 49th Int. Instrumentation Symp. of the ISA (Orlando, FL)* (The International Society of Instrumentation, Systems, and Automation) vol 443
- [23] Jaber A, Zigan L, Sakhrieh A and Leipertz A 2012 Laser-induced phosphorescence in combustion diagnostics: calibration at extremely high temperatures *11th Int. Conf. on Combustion and Energy Utilization (ICCEU)* (Coimbra, Portugal, 9–13 May 2012)
- [24] Jovicic G, Zigan L, Will S and Leipertz A 2015 Luminescence properties of the thermographic phosphors Dy<sup>3+</sup>:YAG and Tm<sup>3+</sup>:YAG for application in high temperature systems *Z. Phys. Chem.* **229** 977–97
- [25] Hertle E, Chepyga L, Batentschuk M and Zigan L 2017 Influence of codoping on the luminescence properties of YAG:Dy for high temperature phosphor thermometry *J. Lumin.* **182** 200–7
- [26] Kwong W, Steinberg A and Chin Y 2014 Effect of B<sup>3+</sup>–N<sup>3–</sup> on YAG:Dy thermographic phosphor luminescence *Opt. Lett.* **39** 6166–9
- [27] Kwong W Y 2014 Development of thermographic phosphor diagnostics for gas turbine temperature measurements *Master's Thesis* Institute for Aerospace Studies, University of Toronto, Canada
- [28] Nau P, Yin Z, Lammel O and Meier W 2018 Wall temperature measurements in gas turbine combustors with thermographic phosphors *ASME J. Eng. Gas Turbines Power* **141** 041021 (They test several phosphors and the highest, YAG:Dy, to 1800 K)
- [29] Phosphor Research Society 1999 *Phosphor Handbook* (Boca Raton, FL: CRC Press) p 87
- [30] Eldridge J I 2019 Luminescence decay-based Y<sub>2</sub>O<sub>3</sub>:Er phosphor thermometry: temperature sensitivity governed

- by multiphonon emission with an effective phonon energy transition *J. Lumin.* **214** (<https://doi.org/10.1016/j.jlumin.2019.116535>)
- [31] Heyes A L 2009 On the design of phosphors for high-temperature thermometry *J. Lumin.* **129** 2004–9
- [32] Fonger W H and Struck C W 1970  $\text{Eu}^{+35}\text{D}$  resonance quenching to the charge-transfer states in  $\text{Y}_2\text{O}_2\text{S}:\text{Eu}$ ,  $\text{La}_2\text{O}_2\text{S}:\text{Eu}$ , and  $\text{LaOCl}$  *J. Chem. Phys.* **12** 6364–72
- [33] Li J, Chen F, Liu W, Zhang W, Wang L, Ba X, Zhu Y, Pan Y and Guo J 2012 Co-precipitation synthesis route to yttrium aluminum garnet (YAG) transparent ceramics *J. Eur. Ceram. Soc.* **32** 2971–9
- [34] Lupei A, Lupei V, Gheorghe G, Ikesue A and Enculescu M 2011 Spectroscopic characteristics of  $\text{Dy}^{3+}$  doped  $\text{Y}_3\text{Al}_5\text{O}_{12}$  transparent ceramics *J. Appl. Phys.* **110** 083120
- [35] Hertle E, Chepyga L, Batentschuk M, Will S and Zigan L 2018 Temperature-dependent luminescence characteristics of  $\text{Dy}^{3+}$ -doped in various crystalline hosts *J. Lumin.* **204** 64–74
- [36] Dharmiah P, Viswanath C S D, Basavapoornima Ch, Krishnaiah K V, Jayasankar C K and Hong S-J 2016 Luminescence and energy transfer in  $\text{Dy}^{3+}/\text{Tb}^{3+}$  co-doped transparent oxyfluorosilicate glass-ceramics for green emitting applications *Mater. Res. Bull.* **83** 507–14
- [37] Chen X, Ma E and Liu G 2007 Energy levels and optical spectroscopy of  $\text{Er}^{3+}$  in  $\text{Gd}_2\text{O}_3$  nanocrystals *J. Phys. Chem. C* **111** 10404–11
- [38] Anderson B, Livers S, Gunawidjaja R and Eilers H 2019 Fiber-based optical thermocouples for fast temperature sensing in extreme environments *Opt. Eng.* **58** 097105